Cellulose nanofiber-templated three-dimension TiO_2 hierarchical nanowire network for photoelectrochemical photoanode

2014 Nanotechnology 25 504005

(http://iopscience.iop.org/0957-4484/25/50/504005)

IOP Publishing Nanotechnology
Nanotechnology **25** (2014) 504005 (10pp) doi:10.1088/0957-4484/25/50/504005

Cellulose nanofiber-templated three-dimension TiO_2 hierarchical nanowire network for photoelectrochemical photoanode

Zhaodong Li[1], Chunhua Yao[1], Fei Wang[1], Zhiyong Cai[3] and Xudong Wang[1,2]

[1] Department of Materials Science and Engineering, University of Wisconsin-Madison, Madison, WI 53706, USA
[2] Beijing Institute of Nanoenergy and Nanosystems, Chinese Academy of Sciences, Beijing 100083, People's Republic of China
[3] Forest Products Laboratory, USDA Forest Service, Madison, WI 53726, USA

E-mail: xudong@engr.wisc.edu and zcai@fs.fed.us

Received 29 June 2014, revised 23 August 2014
Accepted for publication 5 September 2014
Published 26 November 2014

Abstract

Three dimensional (3D) nanostructures with extremely large porosity possess a great promise for the development of high-performance energy harvesting and storage devices. In this paper, we developed a high-density 3D TiO_2 fiber-nanorod (NR) heterostructure for efficient photoelectrochemical (PEC) water splitting. The hierarchical structure was synthesized on a ZnO-coated cellulose nanofiber (CNF) template using atomic layer deposition (ALD)-based thin film and NR growth procedures. The tubular structure evolution was in good agreement with the recently discovered vapor-phase Kirkendall effect in high-temperature ALD processes. The NR morphology was formed via the surface-reaction-limited pulsed chemical vapor deposition (SPCVD) mechanism. Under Xenon lamp illumination without and with an AM 1.5G filter or a UV cut off filter, the PEC efficiencies of a 3D TiO_2 fiber-NR heterostructure were found to be 22–249% higher than those of the TiO_2-ZnO bilayer tubular nanofibers and TiO_2 nanotube networks that were synthesized as reference samples. Such a 3D TiO_2 fiber-NR heterostructure offers a new route for a cellulose-based nanomanufacturing technique, which can be used for large-area, low-cost, and green fabrication of nanomaterials as well as their utilizations for efficient solar energy harvesting and conversion.

Keywords: atomic layer deposition, cellulose nanofiber, 3D structure

(Some figures may appear in colour only in the online journal)

1. Introduction

Photoelectrochemical (PEC) water splitting has received considerable attention in the development of solar fuel technologies to relieve our dependence on fossil fuels and to reduce greenhouse gas emissions [1–4]. High-performance photoelectrodes of PEC systems demand broad-band and high-percentage light absorption; instantaneous and low-loss charge separation, collection and transportation; and large and clean electrode—electrolyte interfaces [4–11]. Three-dimensional (3D) branched nanowire (NW)/nanorod (NR) architectures are considered to be excellent candidates for PEC photoelectrode development. They are composed of highly conductive core NWs that are fully covered with dense and active NR branches [10, 12–16]. Their high performance is a result of their extremely large surface area density, long optical paths, and the potential to achieve rapid photo-generated electron-hole separation and transport. Our recent

development of a surface-reaction-limited pulsed chemical vapor deposition (SPCVD) technique, as a derivative of atomic layer deposition (ALD), enabled uniform growth of high-density NR branches on ultra-compact NW arrays, which led to significant performance gain in solar energy conversion [10, 12].

Natural cellulose-based nanomaterials such as cellulose nanofibers (CNFs) are another type of widely used large-scale renewable 3D mesoporous structures owing to their great abundance, low cost, bio-compatibility, and degradability [17–20]. They are composed of elementary cellulose fibrils and show comparable mechanical properties (e.g., Young's modulus and tensile strength) as other fibrous materials (e.g., carbon fibers and glass fibers) [21]. CNFs also exhibit significant absorbability to both hydrophilic and hydrophobic materials [22]. They are therefore a remarkable template for processing functional 3D nanostructures with extremely large porosity and possess great promise for the development of high-performance energy harvesting and storage devices. For example, nanofibrillated cellulose was utilized as a paper substrate to fabricate thin film transistors achieving high transparency and flexibility of the device [20]; nanostructured networks of cellulose-graphite platelet composites were applied as Li-ion battery anodes, demonstrating excellent flexibility and good cycling performance [23, 24]; porous cellulose-templated TiO_2 nanostructures were used in photocatalytic and dye-sensitized solar cells, exhibiting significantly enlarged surface area and improved electron transport properties [25, 26]; and cellulose/polyaniline nanocomposites were developed for supercapacitors with enhanced mass-specific capacitance [27]. Combining the successful exploration of CNF-templated nanostructures with branched functional NR configurations would lead to a novel hierarchical nanostructure with further enhanced PEC performance and photoelectrode manufacturability. In this paper, we integrated the SPCVD technique for synthesizing high-density TiO_2 NR branches with mesoporous CNF templates. The CNF framework was well preserved under high deposition temperature by introducing ZnO overcoating. The ZnO layer was completely converted into TiO_2 during growth, following the Kirkendall effect [28]. To the best of our knowledge, this is the first time that high density NR branches have been grown into mesoporous CNF networks, which further enlarges the surface area as well as introduces new functionality. Compared to other CNF-templated mesoporous nanostructures (i.e., TiO_2-ZnO bilayer tubular nanofibers networks and TiO_2 nanotubes networks), a 3D TiO_2 fiber-NR heterostructure exhibited significantly enhanced photocurrent and PEC efficiency, owing to their large surface area and good electrical conductivity.

2. Experimental section

2.1. Fabrication of CNF template

The CNFs used in our experiments were tetramethylpiperidine-1-oxy (TEMPO) oxidized wood pulp fibers, which were prepared according to the method reported by Saito *et al* [29, 30]. In particular, the CNFs' hydrogel solution (0.4 wt%) was obtained by mechanically homogenizing the TEMPO-treated wood pulp fibers on an M-110EH-30 Microfluidizer (Microfluidics, Newton, MA, USA) with a series of 200- and 87 μm chambers via two pass-throughs. After printing the CNFs' hydrogel on a fluorine doped tin oxide (FTO) glass substrate, the substrate with hydrogel film was frozen in a liquid N_2 and ethanol bath. The substrate was then placed into the vacuum chamber of a Labconco 4.5 Freeze Dryer (Labconco, Kansas City, MO, USA) immediately, remaining 12 h at room temperature with a base pressure of ~35 mTorr, where sublimation of the ice yielded a nanofibrous structure cellulose film, 10 μm thick on the FTO.

2.2. Fabrication of 3D TiO_2 fiber-NR heterostructure

The as-prepared CNF nanostructures on FTO substrates were loaded into an ALD chamber for ZnO overcoating at 150 °C. In one growth cycle, H_2O and diethylzinc vapor precursors were pulsed into the chamber for 1 s each and separated by N_2 purging for 60 s. The 150-cycle ALD growth yielded a 30 nm-thick ZnO film covering the CNFs. This CNF-ZnO core-shell structure on FTO substrates was then used for SPCVD TiO_2 NR branch growth. Similar to the ALD process, 400 cycles of alternating reactions were conducted at 600 °C. Each cycle consisted of 1 s H_2O pulsing + 60 s N_2 purging + 1 s titanium tetrachloride ($TiCl_4$) pulsing + 60 s N_2 purging. Through this process, TiO_2 NRs were uniformly grown on the fibrous backbones.

In order to compare the PEC performance, both CNF-templated TiO_2-ZnO bilayer tubular nanofibers and fibrous TiO_2 nanotubes networks were prepared. For the TiO_2-ZnO samples, 400 cycles of ALD TiO_2 films were coated on CNF-ZnO core-shell nanofibers. The deposition was performed at 300 °C with 1 s H_2O pulsing + 60 s N_2 purging + 1 s titanium tetrachloride ($TiCl_4$) pulsing + 60 s N_2 purging for each cycle. The fibrous TiO_2 nanotubes network was synthesized via a 400-cycle ALD TiO_2 coating at 150 °C on a CNF template and sintered at 600 °C to crystallize the TiO_2 coating and remove CNF templates [4]. The fabrication processes of three kinds of samples are schematically illustrated in figure 1.

2.3. PEC characterization

PEC characterizations were performed in a 1 mol L^{-1} KOH (pH = 14) aqueous solution using a three-electrode electrochemical cell configuration. The saturated calomel electrode (SCE) was used as the reference electrode, and a Pt wire was used as the counter electrode. All electrodes were connected to a potentiostat system (Metrohm Inc., Riverview, FL) for *J*–*V* measurement. Light illumination was provided by a 150 W Xe arc lamp (Newport Corporation, Irvine, CA), and the intensity at the PEC anode position was adjusted to be 100 mW cm^{-2}. An AM 1.5G filter and a UV cutoff filter were also utilized with the lamp for PEC characterizations.

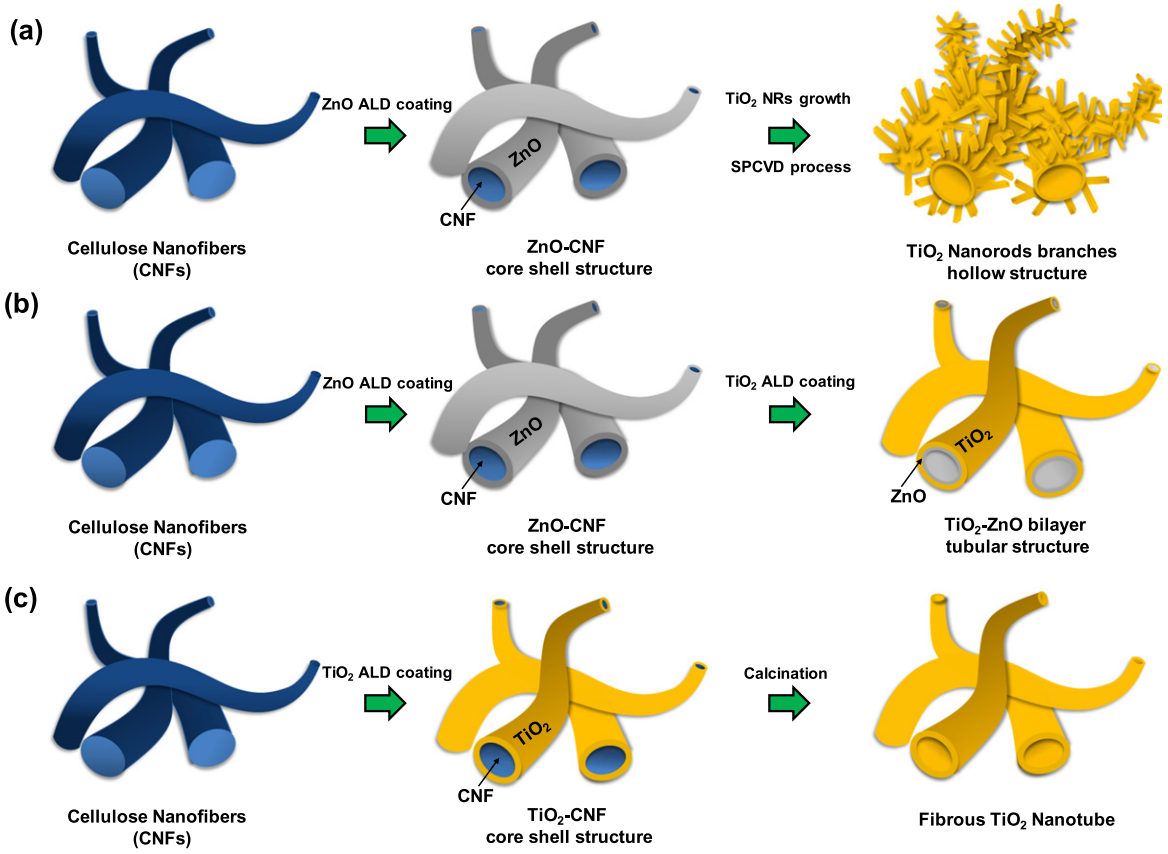

Figure 1. Schematic synthesis procedures of CNF-templated nanostructures. (a) 3D TiO_2 fiber-NR heterostructure by ALD and SPCVD process. (b) TiO_2-ZnO bilayer tubular nanofibers by ALD ZnO and TiO_2 coating. (c) Fibrous TiO_2 nanotubes networks by ALD TiO_2 coating and calcination in vacuum.

3. Results and discussion

The as-fabricated CNF networks on FTO substrates are shown by scanning electron microscopy (SEM) in figure 2(a). The higher-magnification inset reveals a 3D fibrous structure of CNFs with an average fiber diameter of ~0.1 μm. This high-porous nanostructure was well preserved after 150 °C ALD of ZnO thin film conformal coating (figure 2(b)). The surface of the ZnO-coated CNF was relatively rough, which is a result of the polycrystalline nature of the ZnO coating (Inset of figure 2(b)). Figures 2(c) and (d) show the morphologies of the TiO_2-ZnO bilayer tubular nanofibers and the TiO_2 nanotube fibrous networks, respectively, as two reference samples. Both structures present a well-preserved nanofibrous structure. The 300 °C TiO_2 ALD coating yielded a polycrystalline TiO_2 shell over the CNF-ZnO core–shell fibers and burned away the CNF templates (inset of figure 2(c)) [4, 31]. The fiber diameter was slightly increased (~190 nm). The rough surface of the final fibrous structure was replicated from the polycrystalline ZnO and became more notable. The TiO_2 nanotubes shown in figure 2(d) and inset demonstrated a smooth surface with a mean diameter similar to those of the fibrous CNF-ZnO core–shell network. It is noteworthy in figure 2 that the fibrous 3D network configuration was very stable during both low-temperature ALD and high-temperature heat treatment processes, and no morphology change could be observed.

Branched TiO_2 NR SPCVD growth was conducted on the ZnO-coated CNF templates shown in figure 2(b). The 3D fibrous network morphology was also well preserved after 14 h of the 600 °C SPCVD process (figure 3(a)). From higher magnification SEM images, the uniform and dense coverage of TiO_2 NRs can be clearly observed along the entire fiber length (figure 3(b)). The fibers' trunks were ~220 nm in diameter, which was ~22% more than that of the ZnO-CNF template. All TiO_2 NRs were rooted on the walls of nanofibers and pointed out divergently. The NRs exhibited an average length of ~170 nm and a diameter of ~30 nm (aspect ratio is ~5.7) (figure 3(c)). The cross-sectional image of a single fiber (figure 3(d)) shows the hollow center of the branched structure and evidences the removal of fiber templates during high-temperature deposition. The diameter of the orifice was close to 180 nm, which was larger than the size of the cellulose fiber but comparable to that of the CNF-ZnO core-shell template. The continuous wall thickness was only ~10 nm.

The crystal structures of these three CNF-templated TiO_2 fibrous networks were further investigated by transmission electron microscopy (TEM) (figure 4). All the tubular nanofibers exhibited a uniform wall thickness along the entire channel, which is consistent with the SEM results. TiO_2 NR-

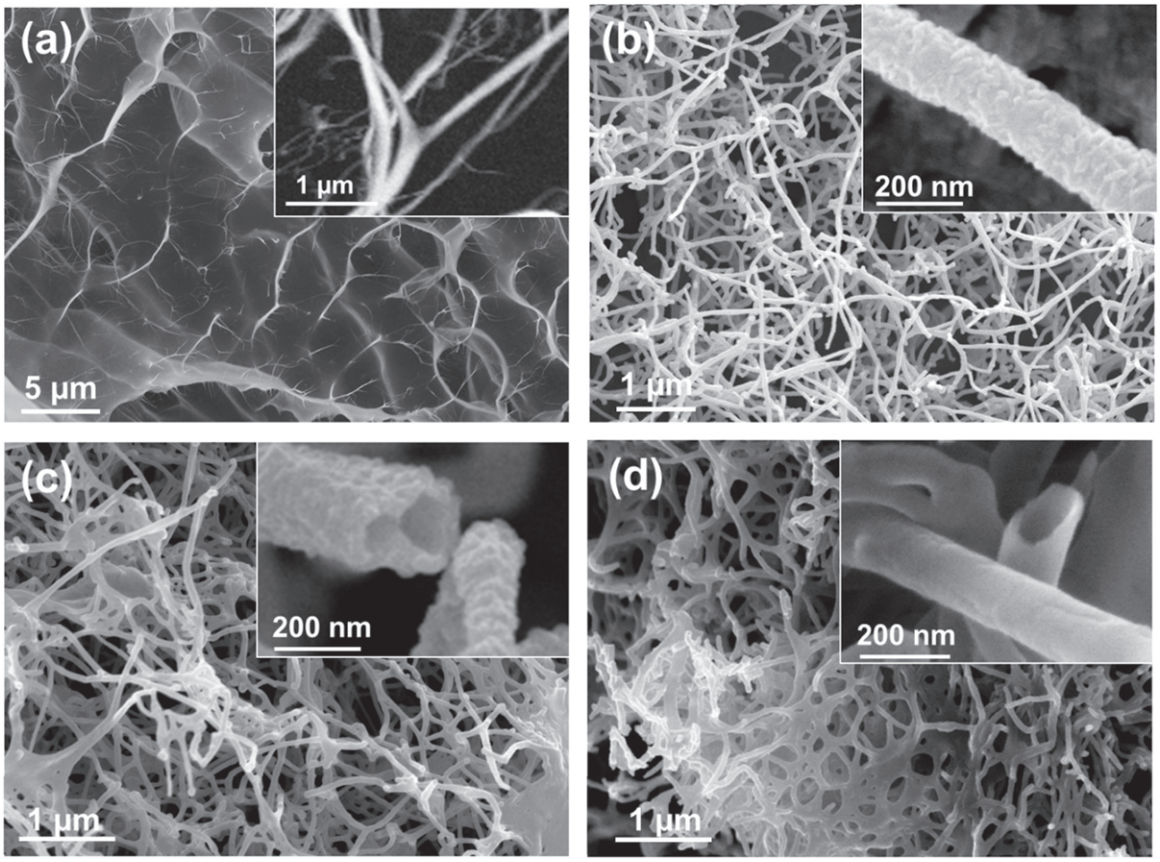

Figure 2. Morphologies and structures of CNF films and templated 3D architectures. (a) CNF film processed on a FTO substrate; inset is a high magnification image for cellulose nanofibers. (b) CNFs coated with 150-cycle ALD ZnO at 150 °C; inset shows the crystalline ZnO film with rough surface. (c) Crystalline TiO_2 film overcoating on CNF-ZnO core–shell template by 300-cycle ALD at 300 °C; inset show the CNF's extinction and nanotubular structure. (d) Fibrous TiO_2 nanotube network after 400-cycle TiO_2 ALD at 150 °C and 24 h annealing at 600 °C in vacuum; inset reveals the hollow structure and related smooth surface.

branched nanofibers are shown in figure 4(a), where a uniform ∼10 nm wall can be clearly observed, and the inner diameter is as large as that of the CNF-ZnO core-shell template. The NRs exhibited a uniform contrast, indicating their single crystal structure. These observations are consistent with our recent discovery of the Kirkendall effect during high-temperature TiO_2 ALD. When ZnO NW arrays were used as the initial template, the 400-cycle SPCVD of TiO_2 at 600 °C yielded high-density branched TiO_2 NRs on TiO_2 nanotubes that were converted from the ZnO NWs via cation diffusion and exchange. In this process, the ZnO surface was exposed to $TiCl_4$ vapor and quickly converted to TiO_2, yielding $ZnCl_2$ vapor byproduct. The subsequent $TiCl_4$ vapor diffused inward, while the Zn^{2+} and O^{2-} ions diffused outward through the polycrystalline TiO_2 shell on the ZnO surface. Upon the reaction between $TiCl_4$ and ZnO, the ZnO was gradually consumed from the TiO_2/ZnO interface, eventually generating a hollow TiO_2 nanotube [28]. We believe such an effect also applied to our CNF-ZnO core-shell templates, where the ZnO shell was fully converted into the thin TiO_2 walls during the initial growth stage.

The TiO_2-ZnO bilayer tubular nanofibers were fabricated via 150 cycles of ZnO and 400 cycles of TiO_2 ALD at 150 °C and at 300 °C, respectively. The wall thickness of this hierarchical tubular structure was found to be ∼50–60 nm (figure 4(b)), which is consistent with the typical ALD growth rate of ZnO and TiO_2. Unlike the 600 °C growth, the lower temperature (300 °C) inhibited cation diffusion and exchange reactions that are required by the implementation of the Kirkendall effect. Thus, crystalline TiO_2 was simply overcoated on the ZnO surfaces and created a TiO_2-ZnO bilayer tubular structure by only burning off CNF cores. Direct TiO_2 ALD on CNF templates yielded a much smoother tubular structure, as shown in figure 4(c). The wall of TiO_2 nanotubes was fairly uniform with a thickness of ∼40 nm, which is accordant with the typical TiO_2 ALD growth rate. The polycrystalline shell exhibited a much larger grain size (>100 nm) formed from the subsequent high-temperature treatment (600 °C), where the CNF templates were also completely removed. Although CNFs have amorphous and crystalline regions, above microscopic observations they reveal no differences in morphology and crystallinity of either TiO_2 NRs or ZnO or TiO_2 overcoatings along the entire CNF surfaces. The preparation methods and representative morphologies of the three types of samples are summarized in table 1.

Surface area is an important parameter to understand the performance enhancement. Considering that the TiO_2 and

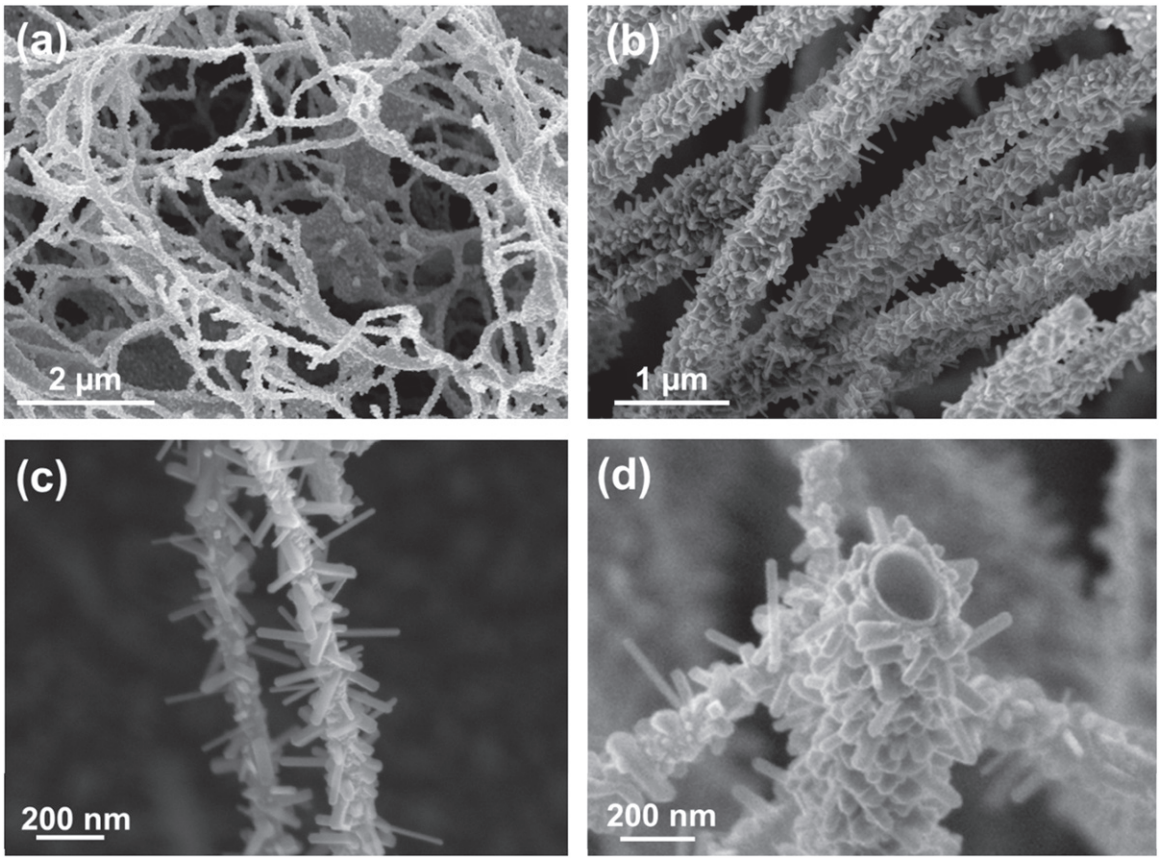

Figure 3. Morphology and structure of CNF-templated TiO_2 branches architecture. (a) Fibrous morphology was preserved after branched TiO_2 network growth. (b) High-density TiO_2 NRs that grew laterally out of the fiber surfaces via 400-cycle SPCVD process. (c) and (d) Higher magnification SEM images indicate entirely covered fiber surfaces with TiO_2 NRs and the hollow backbone structure after growth.

TiO_2/ZnO tubular structures are ALD replicates of the CNF network, they should offer the same surface area as the CNF template (ignoring the small surface reduction due to thickness increase). With NR branches on the TiO_2 shells, the total surface area of such 3D TiO_2 NRs should be higher. Based on the average size and density of the NRs, statistical calculation shows that the surface area of TiO_2 NR-fiber heterostructure is ~950% larger than that of other two samples without NR branches. This surface area enlargement is about the same ratio as growing TiO_2 NRs inside anodized aluminum oxide templates [32].

Elemental and phase information of the three types of fibrous nanostructures were characterized to further confirm the conclusions of structure evolution drawn from the microscopy analyses. From the 3D TiO_2 fiber-NR heterostructure, no Zn signal was detected from the energy-dispersive X-ray spectroscopy (EDS) spectrum (figure 5(a)), nor can the ZnO phase be identified by the X-ray diffraction (XRD) pattern (figure 5(b)). This verifies the fact that all ZnO shells were consumed and replaced by TiO_2 nanotube backbones during NR integration via the Kirkendall effect. From the XRD profile, rutile TiO_2 was identified, which was believed to be a result of the lower anatase phase stability when a foreign element (e.g., Zn) was involved during the growth [33]. As expected, the TiO_2-ZnO bilayer tubular nanofibers showed a strong Zn signal in the EDS spectrum, and the ZnO phase can be clearly identified in the XRD pattern. Due to the existence of Zn elements, the rutile phase also appeared rather than the pure anatase phase from the 300 °C ALD TiO_2 in our earlier publication [10]. The EDS and XRD results of the TiO_2 nanotube network were identical to typical ALD results as shown in our previous work [4], where only anatase TiO_2 was observed. Notably, the EDS analysis showed a distinct C signal from each sample. The amount of carbon preserved in the final products of the TiO_2 fiber-NR heterostructure, TiO_2-ZnO bilayer tubular nanofibers, and TiO_2 nanotube network was identified to be ~6.2%, 7.9%, and 14.4%, respectively. Exposures of H_2O vapor during the 600 °C TiO_2 NR and 300 °C TiO_2 film growth might provide an oxidation environment and lessen the amount of reserved carbon from CNF calcination.

Due to the long optical paths and possible high quality transport channels for rapid charge separation and conduction, as well as the prominent electrolyte—semiconductor interface areas, the 3D TiO_2 fiber-NR heterostructure could be a promising mesoporous configuration for high-performance PEC photoanodes [4, 10, 12, 14, 34, 35]. Such potential merits were explored by conducting PEC water splitting measurements. For performance comparison, the other two samples (TiO_2-ZnO bilayer tubular nanofibers and TiO_2 nanotube networks) were applied as PEC photoanodes as well. The photocurrent density (J_{ph}) versus bias potential characteristics

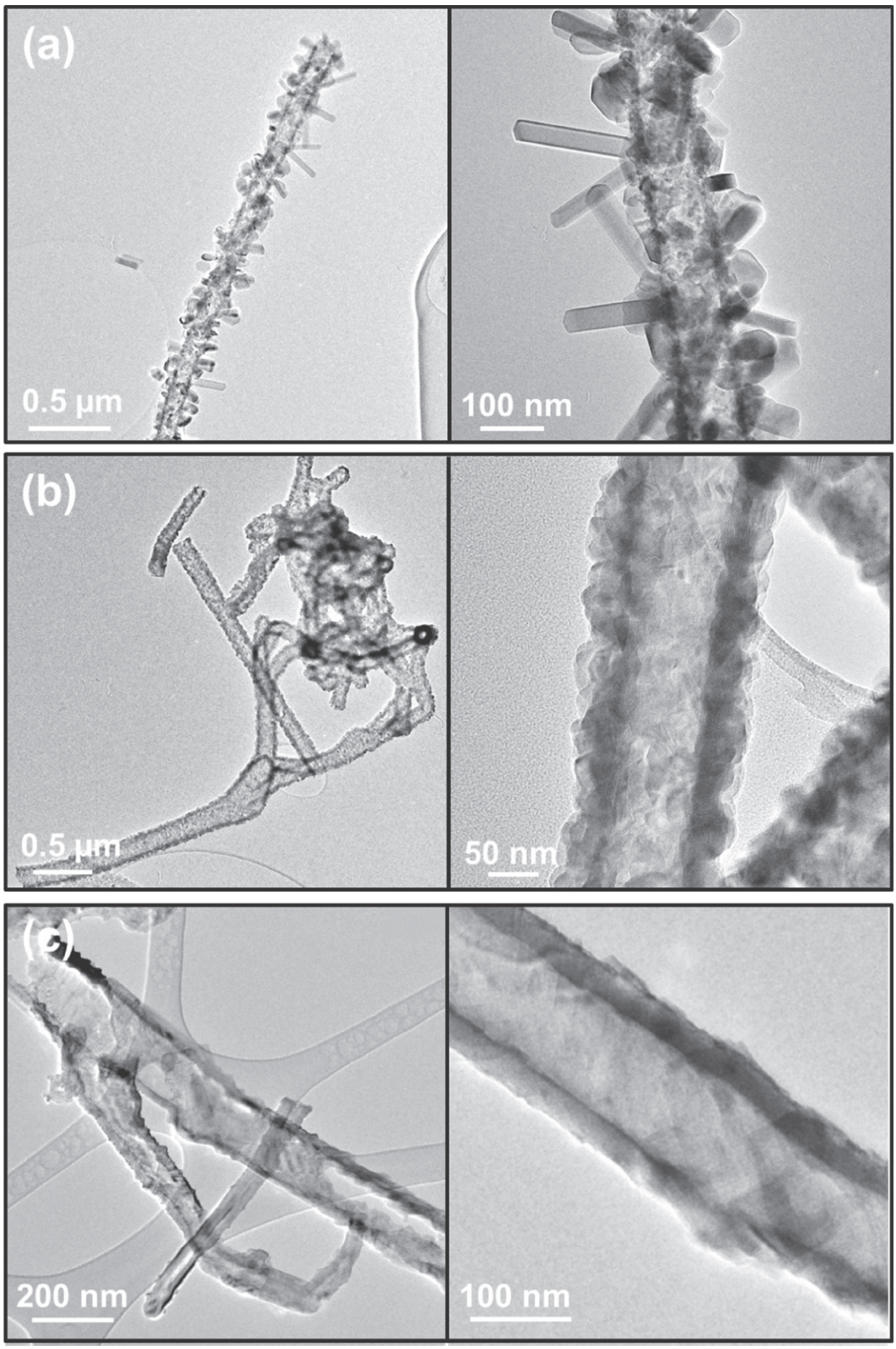

Figure 4. TEM characterizations for different CNF-templated 3D architectures. (a) TiO_2 fiber-NR heterostructure, the nanotubular structure, and TiO_2 NRs with average size of ~170 nm in length and ~30 nm in diameter. (b) TiO_2-ZnO bilayer tubular nanofibers and polycrystalline feature on the surface. (c) Fibrous TiO_2 nanotube structure with uniform wall thickness of TiO_2 and large crystalline domain area.

Table 1. Summary of preparation methods and representative morphologies of the three types of CNF-templated samples.

CNF-templated Sample	Preparation Method	Representative Morphology
TiO_2 fiber-NR heterostructure	ZnO ALD coating on CNFs and then TiO_2 NR growth by SPCVD	TiO_2 NRs rooted on the TiO_2 tubular nanofibers
TiO_2-ZnO bilayer tubular NFs	ZnO ALD coating on CNFs and then crystalline TiO_2 ALD coating	TiO_2 and ZnO double-layer with rough surfaces and hollow cores following the same shape of the CNF template
TiO_2 nanotube networks	Amorphous TiO_2 ALD coating and then annealing	Polycrystalline TiO_2 nanotubes with the same shape as the CNF templates

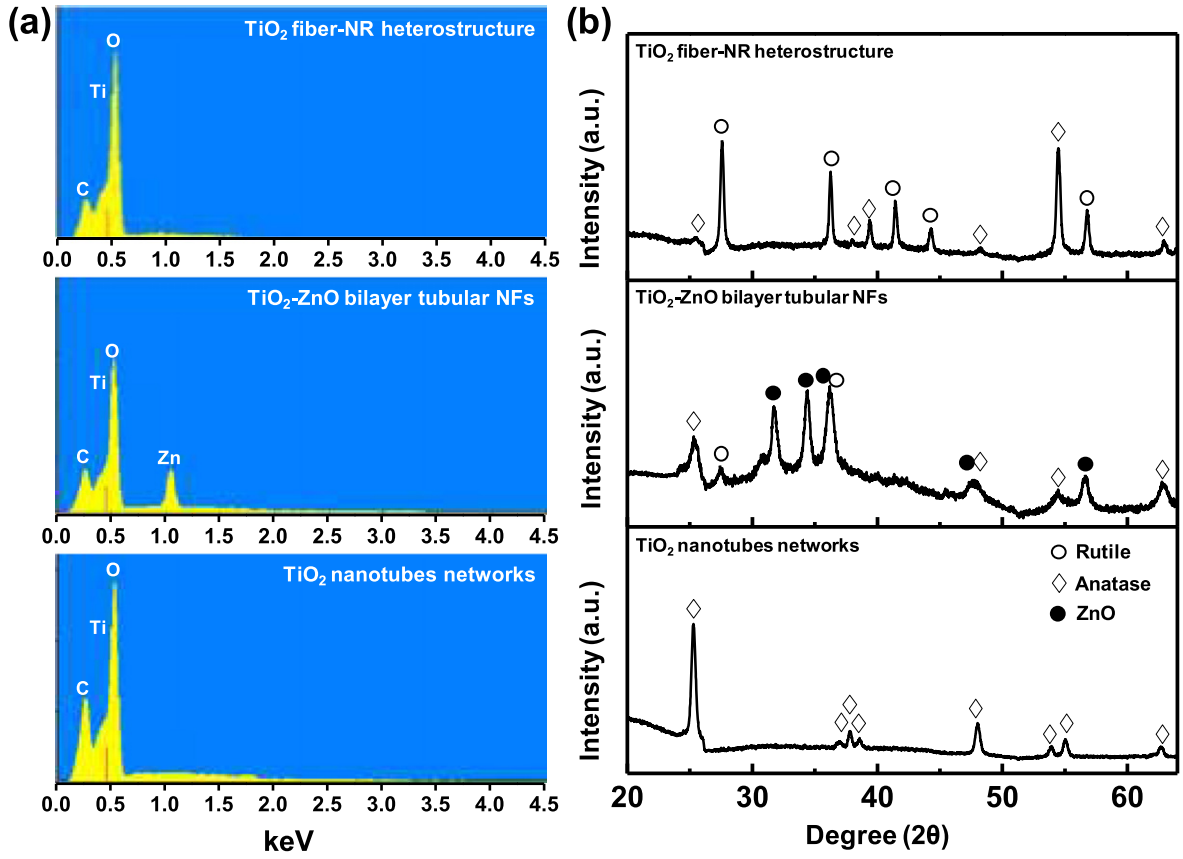

Figure 5. EDS (a) and XRD (b) spectra of TiO_2 fiber-NR heterostructure (top panel), TiO_2-ZnO bi-layer tubular NFs (middle panel), and TiO_2 nanotube networks (bottom panel).

of these three kinds of samples was measured under the same conditions. All the samples were very stable during the PEC test, and no mechanical damages could be observed after the test. The nanostructures can be reused for the measurement without noticeable performance degradation. Corresponding PEC efficiencies were estimated using the following equation [4]:

$$\eta\% = \left[J_{ph}\left(E^0_{rev} - \left|E_{bias} - E_{aoc}\right|\right)\frac{100}{I_0} \qquad (1)$$

where E_{bias} is the bias potential; $E^0_{rev} = 1.23$ V is the standard state reversible potential for the water-splitting reaction; and $E_{aoc} = V_{oc}$ is the open circuit voltage (versus SCE).

The representative $J_{ph} - V$ curves are shown in figure 6(a) under the illumination of a 100 W cm^{-2} Xe lamp source without and with AM 1.5G or UV cutoff filters. The dark current densities of each PEC test remained at fairly small values (<10^{-4} mA cm^{-2}) within the bias potential range scanned between −0.9 V–0.5 V (versus SCE), indicating high quality crystal surfaces of the as-synthesized fibrous networks. In general, the 3D TiO_2 fiber-NR heterostructure exhibited high J_{ph} and efficiency under all wavelength conditions, where the highest values were obtained from the Xe lamp illumination and the lowest values when a UV cutoff filter was applied. Under the Xe lamp, the maximum efficiency was calculated to be 1.13% at ∼ −0.31 V. The maximum efficiency dropped to 0.76% at ∼ −0.26 V for the AM 1.5G filter and 0.17% at ∼ −0.35 V for the UV cutoff filter (figure 6(b)). This phenomenon evidences that the performance of TiO_2 nanostructure-based photoanodes was mainly governed by UV absorption. Nevertheless, appreciable PEC performance was achieved when only visible light was

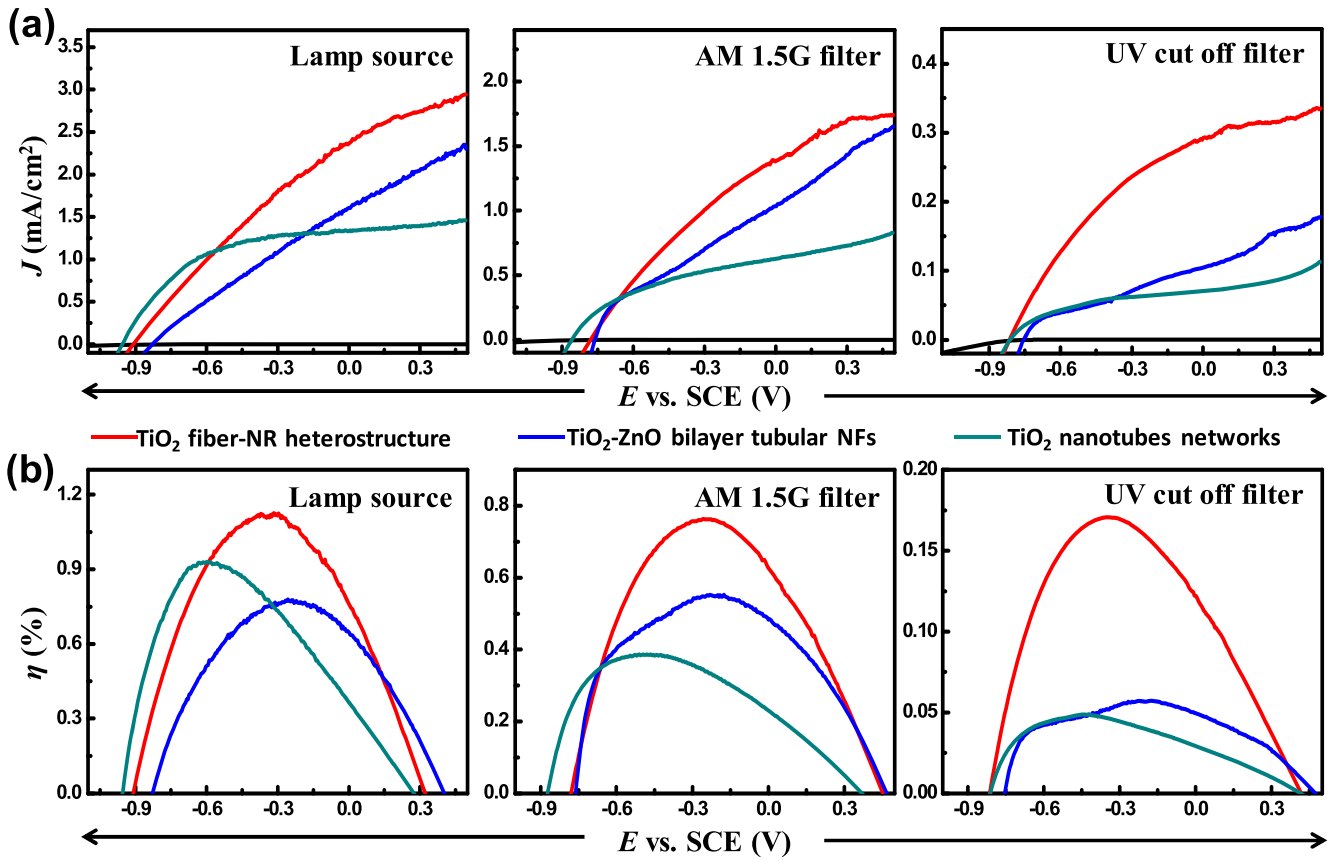

Figure 6. (a) Photoelectrochemical performance of three CNF-templated fibrous networks under illuminations of a 100 mW cm^{-2} Xe lamp source, a lamp with an AM 1.5G filter, and with a UV cutoff filter. (b) Corresponded PEC efficiencies for these CNF-templated 3D architectures.

illuminated. The photoactivity in the visible light region can be attributed to the presence of carbon elements as discovered in our recent study [4].

Compared to the other two reference samples, the J_{ph} of 3D TiO_2 fiber-NR heterostructures exhibited obviously higher values under all illumination wavelength ranges. When illuminated directly under the Xe lamp, maximum efficiency (1.13% at ~ −0.31 V) is 45% and 22% higher than that of the TiO_2-ZnO bilayer tubular nanofibers (0.78% at ~ −0.26 V) and TiO_2 nanotube networks (0.93% at ~ −0.6 V), respectively (figure 6(b)). When the AM1.5G and UV cut-off filters were applied, the TiO_2 fiber-NR heterostructure exhibited even higher advantages compared to the other two. Under AM1.5G illumination, its maximum efficiency was 38% and 97% higher than that of the TiO_2-ZnO bilayer tubular nanofibers and TiO_2 nanotube networks, respectively. Under only visible light, the enhancement was raised to 195% and 249% as compared to the TiO_2-ZnO bilayer tubular nanofibers and TiO_2 nanotube networks, respectively. The largest surface area is generally believed to be the main reason for the enhanced performance. However, the much more significant enhancement in the visible light region suggests that the charge transport might be the bottleneck when a higher flux photogenerated charge was induced. This argument can also be supported by the shapes of $J_{ph}-V$ characteristics. As shown in figure 6(a), the saturation regions of both the TiO_2 fiber-NRs heterostructure and the TiO_2-ZnO bilayer tubular nanofiber samples were less obvious, indicating the existence of a larger number of defects and grain boundaries in these two samples acting as the recombination sites, which jeopardizes the separation and transport of photogenerated charges [36, 37].

4. Conclusion

In this work, we developed a high-density 3D TiO_2 fiber-NR heterostructure for efficient PEC photoanodes. A 3D CNF network with ZnO shells was used as a template for SPCVD growth of TiO_2 NR branches. The ZnO layer interacted with $TiCl_4$ vapor and was quickly converted into polycrystalline TiO_2 thin films, seeding the growth of TiO_2 NRs. The template dimension and 3D morphology were well preserved. The structure evolution was in good agreement with the vapor-phase Kirkendall effect in ALD system that we discovered recently. The 3D fiber-NR heterostructure offers large porosities and tremendous surface areas for PEC water splitting. Its PEC efficiency was found to be 22%–249% higher than those of the TiO_2-ZnO bilayer tubular nanofibers and TiO_2 nanotube networks that were synthesized as reference samples. The much more conspicuous photoactivity in longer wavelength regions, together with the $J_{ph}-V$

characteristics, suggest that charge transport might be the issue for the 3D fiber-NR heterostructure to further enhance its PEC performance. This technique opens a new avenue toward a cellulose-based nanomanufacturing technique, which holds great promise for large-area, low-cost, and green fabrication of functional nanomaterials, as well as their applications in solar energy harvesting and conversion areas.

Acknowledgments

Research was primarily supported by the US Department of Energy (DOE), Office of Science, Basic Energy Sciences (BES), under Award # DE-SC0008711. CY thanks the support of the National Science Foundation under Award CMMI-1233570.

References

[1] Maeda K and Domen K 2010 Photocatalytic water splitting: recent progress and future challenges *J. Phys. Chem. Lett.* **1** 2655–61

[2] Su J, Feng X, Sloppy J D, Guo L and Grimes C A 2011 Vertically aligned WO(3) nanowire arrays grown directly on transparent conducting oxide coated glass: synthesis and photoelectrochemical properties *Nano Lett.* **11** 203–8

[3] Chen X, Shen S, Guo L and Mao S S 2010 Semiconductor-based photocatalytic hydrogen generation *Chem. Rev.* **110** 6503–70

[4] Li Z, Yao C, Yu Y, Cai Z and Wang X 2014 Highly efficient capillary photoelectrochemical water splitting using cellulose nanofiber-templated TiO_2 photoanodes *Adv. Mater.* **26** 2262–7 110

[5] Yin W-J, Tang H, Wei S-H, Al-Jassim M M, Turner J and Yan Y 2010 Band structure engineering of semiconductors for enhanced photoelectrochemical water splitting: the case of TiO_2 *Phys. Rev.* B **82** 045106

[6] Hwang Y J, Boukai A and Yang P 2009 High density n-Si/n-TiO_2 core/shell nanowire arrays with enhanced photoactivity *Nano Lett.* **9** 410–5

[7] Boettcher S W, Spurgeon J M, Putnam M C, Warren E L, Turner-Evans D B, Kelzenberg M D, Maiolo J R, Atwater H A and Lewis N S 2010 Energy-conversion properties of vapor-liquid-solid-grown silicon wire-array photocathodes *Science* **327** 185–7

[8] Kim J-H, Yun T K, Bae J-Y and Ahn K-S 2009 Enhanced carrier transport of N-doped TiO_2 for photoelectrochemical cells *Japan. J. Appl. Phys.* **48** 120204

[9] Shen X, Sun B, Yan F, Zhao J, Zhang F, Wang S, Zhu X and Lee S 2010 High-performance photoelectrochemical cells from ionic liquid electrolyte in methyl-terminated silicon nanowire arrays *ACS Nano* **4** 5869–76

[10] Shi J, Hara Y, Sun C, Anderson M A and Wang X 2011 Three-dimensional high-density hierarchical nanowire architecture for high-performance photoelectrochemical electrodes *Nano Lett.* **11** 3413–9

[11] Wang F, Seo J H, Li Z, Kvit A V, Ma Z and Wang X 2014 Cl-doped ZnO nanowires with metallic conductivity and their application for high-performance photoelectrochemical electrodes *ACS Appl. Mater. Interfaces* **6** 1288–93

[12] Shi J and Wang X 2012 Hierarchical TiO_2–Si nanowire architecture with photoelectrochemical activity under visible light illumination *Energy Environ. Sci.* **5** 7918

[13] Cho I S, Chen Z, Forman A J, Kim D R, Rao P M, Jaramillo T F and Zheng X 2011 Branched TiO_2 nanorods for photoelectrochemical hydrogen production *Nano Lett.* **11** 4978–84

[14] Kargar A, Sun K, Jing Y, Choi C, Jeong H, Jung G Y, Jin S and Wang D 2013 3D branched nanowire photoelectrochemical electrodes for efficient solar water splitting *ACS Nano* **7** 9407–15

[15] Cheng C and Fan H J 2012 Branched nanowires: synthesis and energy applications *Nano Today* **7** 327–43

[16] Luo J, Ma L, He T, Ng C F, Wang S, Sun H and Fan H J 2012 TiO_2/(CdS, CdSe, CdSeS) nanorod heterostructures and photoelectrochemical properties *J. Phys. Chem.* C **116** 11956–63

[17] Zeng J, Li R, Liu S and Zhang L 2011 Fiber-like TiO_2 nanomaterials with different crystallinity phases fabricated via a green pathway *ACS Appl. Mater. Interfaces* **3** 2074–9

[18] Liu S, Tao D, Bai H and Liu X 2012 Cellulose-nanowhisker-templated synthesis of titanium dioxide/cellulose nanomaterials with promising photocatalytic abilities *J. Appl. Polym. Sci.* **126** E282–90

[19] Moon R J, Martini A, Nairn J, Simonsen J and Youngblood J 2011 Cellulose nanomaterials review: structure, properties and nanocomposites *Chem. Soc. Rev.* **40** 3941–94

[20] Zhu H, Fang Z, Preston C, Li Y and Hu L 2014 Transparent paper: fabrications, properties, and device applications *Energy Environ. Sci.* **7** 269

[21] Wang B 2008 Dispersion of cellulose nanofibers in biopolymer based nanocomposites *PhD Thesis* University of Toronto, Toronto

[22] Serizawa T, Sawada T, Okura H and Wada M 2013 Hydrolytic activities of crystalline cellulose nanofibers *Biomacromolecules* **14** 613–7

[23] Jabbour L, Gerbaldi C, Chaussy D, Zeno E, Bodoardo S and Beneventi D 2010 Microfibrillated cellulose–graphite nanocomposites for highly flexible paper-like Li-ion battery electrodes *J. Mater. Chem.* **20** 7344

[24] Jabbour L, Destro M, Gerbaldi C, Chaussy D, Penazzi N and Beneventi D 2012 Use of paper-making techniques for the production of Li-ion paper-batteries *Nord. Pulp. Pap. Res. J.* **27** 472–5

[25] Kemell M, Pore V, Ritala M, Leskela M and Linden M 2005 Atomic layer deposition in nanometer-level replication of cellulosic substances and preparation of photocatalytic TiO_2/cellulose composites *J. Am. Chem. Soc.* **127** 14178–9

[26] Ghadiri E, Taghavinia N, Zakeeruddin S M, Gratzel M and Moser J E 2010 Enhanced electron collection efficiency in dye-sensitized solar cells based on nanostructured TiO_2 hollow fibers *Nano Lett.* **10** 1632–8

[27] Wang H H, Zhu E W, Yang J Z, Zhou P P, Sun D P and Tang W H 2012 Bacterial cellulose nanofiber-supported polyaniline nanocomposites with flake-shaped morphology as supercapacitor electrodes *J. Phys. Chem.* C **116** 13013–9

[28] Yu Y, Yin X, Kvit A and Wang X 2014 Evolution of hollow TiO_2 nanostructures via the Kirkendall effect driven by cation exchange with enhanced photoelectrochemical performance *Nano Lett.* **14** 2528–35

[29] Qing Y, Sabo R, Cai Z and Wu Y 2012 Resin impregnation of cellulose nanofibril films facilitated by water swelling *Cellulose* **20** 303–13

[30] Saito T, Hirota M, Tamura N, Kimura S, Fukuzumi H, Heux L and Isogai A 2009 Individualization of nano-sized plant cellulose fibrils by direct surface carboxylation using TEMPO catalyst under neutral conditions *Biomacromolecules* **10** 1992–6

[31] Korhonen J T, Hiekkataipale P, Malm J, Karppinen M, Ikkala O and Ras R H 2011 Inorganic hollow nanotube

aerogels by atomic layer deposition onto native nanocellulose templates *ACS Nano* **5** 1967–74
[32] Shi J, Sun C, Starr M B and Wang X 2011 Growth of titanium dioxide nanorods in 3D-confined spaces *Nano Lett.* **11** 624–31
[33] Shi J A and Wang X D 2011 Growth of rutile titanium dioxide nanowires by pulsed chemical vapor deposition *Cryst. Growth Des.* **11** 949–54
[34] Liu C, Tang J, Chen H M, Liu B and Yang P 2013 A fully integrated nanosystem of semiconductor nanowires for direct solar water splitting *Nano Lett.* **13** 2989–92
[35] Kargar A *et al* 2013 Tailoring n-ZnO/p-Si branched nanowire heterostructures for selective photoelectrochemical water oxidation or reduction *Nano Lett.* **13** 3017–22
[36] Morgan B J and Watson G W 2010 Intrinsic n-type defect formation in TiO_2: a comparison of rutile and anatase from GGA+U calculations *J. Phys. Chem.* C **114** 2321–8
[37] Wu N, Wang J, Tafen de N, Wang H, Zheng J G, Lewis J P, Liu X, Leonard S S and Manivannan A 2010 Shape-enhanced photocatalytic activity of single-crystalline anatase TiO_2 (101) nanobelts *J. Am. Chem. Soc.* **132** 6679–85